ACS SENSORS

Article

Cite This: ACS Sens. 2019, 4, 286–293

pubs.acs.org/acssensors

Attomolar Label-Free Detection of DNA Hybridization with Electrolyte-Gated Graphene Field-Effect Transistors

Rui Campos,[†,∥] Jérôme Borme,[†] Joana Rafaela Guerreiro,[‡] George Machado, Jr.,[†,§] Maria Fátima Cerqueira,[†,§] Dmitri Y. Petrovykh,[‡] and Pedro Alpuim*[,†,§]

[†]Department of Quantum and Energy Materials, International Iberian Nanotechnology Laboratory, 4715-330 Braga, Portugal

[‡]Department of Life Sciences, International Iberian Nanotechnology Laboratory, 4715-330 Braga, Portugal

[§]Center of Physics, University of Minho, 4710-057 Braga, Portugal

Supporting Information

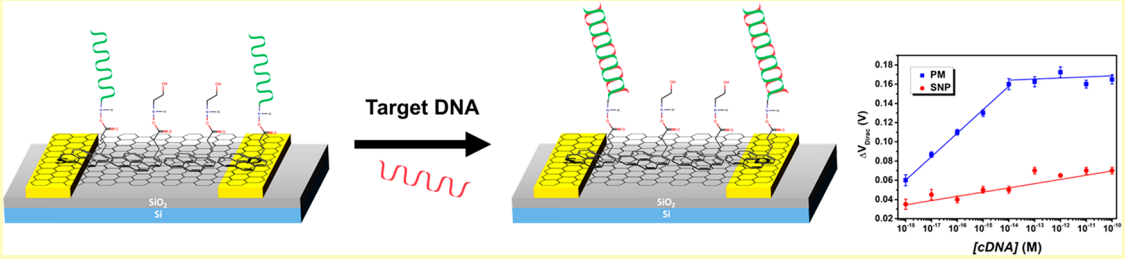

ABSTRACT: In this work, we develop a field-effect transistor with a two-dimensional channel made of a single graphene layer to achieve label-free detection of DNA hybridization down to attomolar concentration, while being able to discriminate a single nucleotide polymorphism (SNP). The SNP-level target specificity is achieved by immobilization of probe DNA on the graphene surface through a pyrene-derivative heterobifunctional linker. Biorecognition events result in a positive gate voltage shift of the graphene charge neutrality point. The graphene transistor biosensor displays a sensitivity of 24 mV/dec with a detection limit of 25 aM: the lowest target DNA concentration for which the sensor can discriminate between a perfect-match target sequence and SNP-containing one.

KEYWORDS: *biosensor, graphene, DNA, EGFET (electrolyte-gated field-effect transistor), planar technology, receded gate transistor, surface functionalization*

DNA detection platforms are developing at a dizzying pace as they provide information for a wide range of fields, including, molecular biology research,[1] genetic disease diagnostics,[2] biological informatics,[3] forensics,[4] and environmental monitoring.[5] Field-effect transistors are an alternative to the common methods for the detection of DNA (polymerase chain reaction (PCR),[6] optical,[7] and electrochemical techniques[7,8]) with the advantage of allowing for high sensitivity, specificity and short measurement time without the need of labeling. Moreover, field-effect transistor (FET) technology lends itself to microfabrication at the wafer scale and, due to the small footprint of the devices, a large number of sensors can be placed in a single chip. Biosensors based on FETs (bio-FETs) are functionalized with a biological recognition element that captures the target molecule, producing an electrostatic gating effect.[9]

The transistor channel in a standard FET, e.g., in the metal-oxide-semiconductor FET (MOSFET), forms at the interface between a bulk semiconductor, e.g., silicon, and a dielectric thin film, e.g., silicon oxide.[10] The semiconductor-dielectric interface is buried inside the device, therefore, the interface is not accessible for functionalization. Consequently, the surfaces for biorecognition are either an extension of the gate contact (like in charge-modulated FETs) or the surface of the gate oxide itself (like in ion-sensitive ISFETs).[11] These surfaces are then exposed to the medium carrying the analyte, and whenever biorecognition events occur, they modulate the gate capacitance and, therefore, the electric field across the gate dielectric resulting from the applied gate voltage. The gate dielectric must be thin, to lower the operating voltage and increase the transconductance, which dictates the device sensitivity, but cannot be so thin as to increase the leakage current beyond acceptable levels or cause electric disruption of the dielectric material. These restrictions limit the sensitivity of bio-FETs based on conventional FET architectures.

Almost all of the above challenges can be addressed more efficiently by a graphene electrolyte-gated FET (EGFET).[12] Because the transistor channel is formed by a one-atom-thick graphene layer, at least one of its surfaces can be left accessible for functionalization. The local gating effect is much more effective than that in conventional devices, because now the charged species modulating the electric field can be directly

Received: April 30, 2018
Accepted: January 23, 2019
Published: January 23, 2019

DOI: 10.1021/acssensors.8b00344
ACS Sens. 2019, 4, 286–293

attached to the transistor channel. And the electrical double layers (EDLs) that form at the graphene−electrolyte and electrolyte−gate contact interfaces, with characteristic thickness given by the Debye length (d_D) (just a few tens of Angstroms thick), replace the solid gate dielectric. The resulting EDL capacitance is huge and allows operating the device at very low gate voltage (V_{GS}), with very high transconductance. Moreover, V_{GS} can be applied in a receded contact, placed far away from the transistor channel, across a vast volume of solution (as compared with the volume defined by the d_D), because the V_{GS} drops essentially in the EDLs.[11,13]

One-dimensional materials, e.g., carbon nanotubes and silicon nanowires, can also be used in high-sensitivity EGFETs[14,15] based on the same working principles, and with similar advantages, but due to the difficulty and cost of large-scale fabrication their use is limited.[9] Besides, control of structural and electronic properties of 1D materials is, so far, elusive, resulting in a large variability in device performance.[16] Two-dimensional materials, compatible with standard planar technology, present themselves as logical alternatives for bio-FET development, with graphene leading the way[15,17,18] for other promising materials.[16,19]

FETs made of single layer graphene (SLG) present better detection limits than those made of graphene oxide or few-layer graphene,[20−22] mainly because they have a much higher transconductance. Zheng et al.[23] showed an improvement, from 100 fM to 10 fM, in the detection limit of PNA/DNA hybridization, when they changed from rGO to chemical vapor deposited (CVD) monolayer graphene.[23,24] Moving from a single graphene FET to an array composed of six CVD graphene FETs, Xu et al.[25] detected DNA hybridization down to 100 fM. Either through direct adsorption of the oligonucleotide on the graphene surface[20,22] or through the use of linkers,[23−27] the reported DNA hybridization detection limits are in the fM range.

EGFETs essentially sense phenomena that occur inside a volume set by the width of the Debye layer. Changing the ionic strength of the buffer, therefore, implies a change in the volume of detection of hybridization events. Higher ionic strength promotes hybridization, since it screens more of the negative charge of the DNA backbone, but lower ionic strength is equivalent to an expanded EDL, with an increased space-charge volume for sensing, and consequently an expanded range of detection of the hybridization process.[25,27] With this in mind Chen et al.[21] used a low-ionic-strength buffer and showed an improvement to the detection limit in the pM range.

Here, we develop a CVD-grown SLG receded-gate field-effect transistor for label-free detection of target DNA with high specificity and ultrahigh sensitivity. The specificity is intrinsic to DNA biorecognition when using a DNA probe perfectly matched to the DNA target, while the sensitivity comes from the transducing capability of the graphene-electrolyte interface of the EGFET. The transistor performance is enhanced by its architecture, with a large-area in-plane gate surrounding the graphene channel placed at its center (the gate area is ≈2500 times larger than the channel area), providing a uniform distribution of the potential inside the water droplet and a very uniform gating field. The large overlap between graphene and gold over the source and drain contacts (overlapping area in each contact is ≈2.35 larger than channel area) provides ohmic contacts. In this way, DNA hybridization is detected down to 25 aM while maintaining the ability to detect single nucleotide polymorphism (SNP) in the DNA target strand.

MATERIALS AND METHODS

Materials. All components of buffer solutions (Na_2HPO_4, NaH_2PO_4, NaCl, $MgCl_2$, 1-Dodecanethiol (DDT) and 1-pyrenebutyric acid succinimidyl ester (PBSE) and all the solvents were from Sigma−Aldrich. Ultrapure water (18 MΩ cm, Millipore, Bedford, MA, USA) was used throughout the experiments. The probe DNA (pDNA), with a 3′ C7-amino modification (5′- TCA TAA CCG GCG AAA GGC TGA AGC T-3′), the complementary DNA (5′-AGC TTC AGC CTT TCG CCG GTT ATG A-3′), the SNP containing target (5′-AGC TTC AGC CTT ACG CCG GTT ATG A-3′) and the probe complementary to the SNP sequence with a 3′ C7-amino modification (5′- TCA TAA CCG GCG TAA GGC TGA AGC T-3′) were synthesized by Metabion International AG, Martinsried, Germany. The melting temperature, T_m, of the DNA duplex was estimated using DINAMelt web server,[28] and was 82.7 °C (80.4 °C for SNP containing duplex and 82.3 °C for the fully complementary SNP) in the hybridization buffer (10 mM PB/150 mM NaCl/50 mM $MgCl_2$) and 58.9 °C (54.8 °C for SNP containing duplex and 58.5 °C for the fully complementary SNP) in the working buffer solution (10 mM PB). High purity (>99.99%) copper foil for graphene growth was purchased from Alfa-Aesar or Goodfellow.

EGFET Fabrication. A detailed procedure is described elsewhere[29,30] and briefly given here. The fabrication of the contacts is performed on 200 mm Si (100) wafer (B-doped, 8−30 Ω, LG Siltron) with 200 nm of thermal oxide. A sputtered layer of Cr 3/Au 30 nm is used as the contact material. The source, drain, and gate contacts are patterned using optical lithography (channel size 25 μm × 75 μm) and then etched by ion milling. A 250 nm multilayer of silicon nitride and silicon oxide is grown by chemical vapor deposition. Optical lithography defines the area of the current lines to be protected by the passivation. Reactive ion etching is used to remove the passivation from outside the current lines. The drain, source and gate contacts are protected with a layer containing aluminum, which stops the reactive ion etch. After etching, the stopping layer is removed by wet etching. A thin aluminum oxide layer (10 nm) is deposited uniformly, and patterned by optical lithography and wet etching to open the channel, source and drain contacts. Graphene is then transferred. Photoresist is spun and patterned by optical lithography to protect the area of the source, drain, and channel. Oxygen plasma is used to etch the graphene. The aluminum oxide layer is removed using wet etching. The wafer is then coated with photoresist as a protection and diced into individual dies.

Graphene Growth and Transfer. Single-layer graphene is grown by thermal chemical vapor deposition on high purity copper foils. The copper foil is cut into 10 cm × 10 cm parts and fit into a graphite confinement box which isolates the substrate from sources of contamination. The substrate is introduced into a three zone quartz tube furnace (EasyTube ET3000, CVD Corp.) and first annealed at 1020 °C for 20 min in hydrogen atmosphere (300 sccm, 0.5 Torr). The gaseous carbon source is a mixture of methane and hydrogen (H_2:CH_4 6:1, 0.5 Torr) that flows into the furnace for 30 min, while keeping the temperature at 1020 °C. After growth, graphene is transferred by a standard procedure using a PMMA temporary substrate (see the Supporting Information (SI)).

Transistor Architecture. The transistor architecture is planar, with a receded gate.[30] The source and drain are two semicircular contacts of 75 μm of diameter, separated by a 25 μm gap which constitutes the graphene channel (see Figure 1). A concentric two-lobe annular gate is placed at 50 μm distance from source and drain. The total gate diameter is 3 mm and presents an area that is 2480 times larger than the channel area.

EGFET Functionalization with DNA. The fabricated chips, protected with photoresist for the dicing, were washed with acetone and then immersed in ethyl acetate for 2 h. The development of the DNA biosensor is schematically illustrated in Figure S1 in the SI. The Au receded gate is passivated with DDT[31] (overnight, 2 mM ethanol

DOI: 10.1021/acssensors.8b00344
ACS Sens. 2019, 4, 286−293

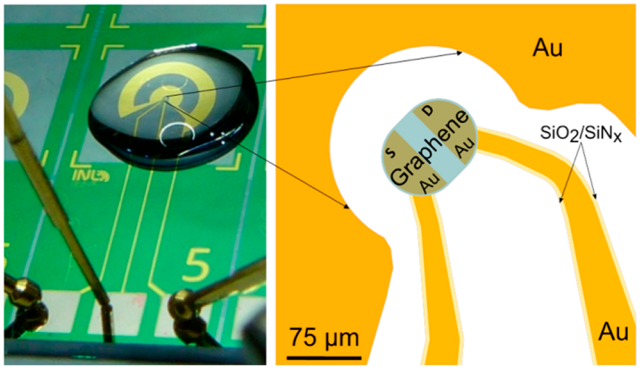

Figure 1. (left) Optical image of one transistor chip under measurement; (right) drawing of the transistor zoomed-in channel region, showing source (S), drain (D), gate (partial view), channel, and Au contact lines with SiO_2/SiN_x passivation layer.

solution) to avoid adsorption of DNA on the Au surface (stage 1). Au source and drain contact areas that may be exposed due to discontinuities in the graphene layer covering them, are also passivated in this stage. In stage 2, the graphene surface is functionalized with PBSE[32] (immersion in 10 μL of a 10 mM solution in dimethylformamide (DMF), for 2 h, followed by rinsing with DMF, H_2O and drying with N_2). The PBSE molecule contains a pyrene group that binds to graphene via $\pi-\pi$ interaction, and an ester group at the other end, which reacts with primary amines. Probe DNA is immobilized by NHS reaction by placing a 10 μL drop of 10 μM pDNA in buffer (overnight, in wet chamber at 4 °C) on the graphene surface modified with PBSE. The last step (stage 4) before target DNA detection (stage 5) is the passivation of the graphene surface with ethanolamine (10 μL of 100 mM solution in 10 mM PB, pH 8.5, 30 min[33]) which reacts with the molecules of PBSE that did not react with the DNA probes.

RESULTS AND DISCUSSION

The EGFETs used here were fabricated at the 200 mm wafer scale, with multiple chips in each wafer. An optical image of an EGFET is shown in Figure 1, with the source, drain, and gate contacts clearly visible. The transistor channel is at the center of the surrounding two-lobed annular gate, providing a uniform distribution of the electric potential in the vicinity of the channel. The large overlap area between graphene and Au over the entire source and drain surface makes good ohmic contacts to the channel. Graphene coverage of the source and drain Au contacts, prevents the Au surfaces from exposure to the solutions and biomolecules contained therein, which renders the measurements more reliable. After fabrication, the wafer is diced into individual chips that are used for the biosensor development.

DNA Biosensor Development. Transfer curves, TCs, i.e., records of the drain-source current, I_{DS}, under constant drain-source voltage, V_{DS}, as a function of the gate-source voltage, V_{GS}, were acquired after each stage of the biosensor development process (top lines in Figures 2 and S2). Raman spectra were acquired after stages 0 (as-fabricated), 1, 2, and 5 (see Materials and Methods and Figure S1 in the SI, where these steps are schematically illustrated). All the TCs were measured in 10 mM phosphate buffer (PB), and, in stage 0, also in ultrapure water (resistivity of 18 MΩ cm), while Raman spectra were acquired on dried samples. Concerning the TC measurements, most devices presented some drift in their TCs when measured repeatedly (Figures S2 and S3, Supporting Information), especially during the first few repetitions.

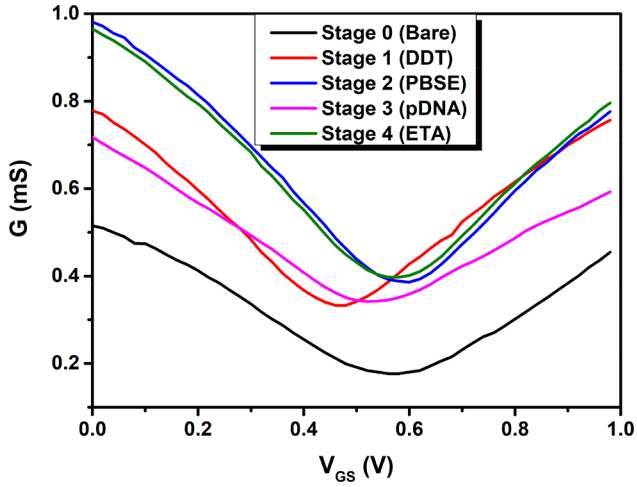

Figure 2. Characteristic transfer curves after each stage of the EGFET channel functionalization.

Therefore, each measurement was repeated 10 times and the data presented in the following sections correspond to the tenth curve acquired in each series of measurements. Each measurement was repeated on five different sensors; hence the results shown are an average of five independent measurements. The complete set of TCs for all the stages and different concentrations can be found in Figure S2, Supporting Information.

At stage 0, the TC (Figure 2, black line) shows the typical ambipolar character of a graphene FET. The curve is symmetric around a point of minimum I_{DS}, occurring at a gate voltage V_{Dirac}, where the channel conductivity is at its lowest, corresponding to an electron chemical potential (Fermi level) as close as it can be practically realized to the Dirac point.[34] The steep branches in the curve, to the left and right of V_{Dirac}, correspond to transport by holes and electrons, respectively. The position of V_{Dirac}, shifted to positive values of gate voltage, shows that our graphene is p-doped. This unintentional doping likely originates from residues of process chemicals and is common in CVD-graphene processed by wet transfer.[35]

Nucleic acids adsorb easily onto gold surfaces,[36,37] so the passivation of the Au gate is an important step for preventing the adsorption of both the probe and target DNA sequences on its surface and producing measurement artifacts. The passivation was done in stage 1 (Figure S1) and the TC measurement after this stage leads to a shift of -100 ± 40 mV in V_{Dirac} (Figure 2, red curve). The shift results from a change of composition of the gate surface, with the formation of a dense self-assembled monolayer (SAM) that covers the Au contact.[21] This process is accompanied by dipole formation at the interface, induced by charge transfer during chemisorption of S on Au and the combined dipole moments of the alkane chains. For common alkanethiols, like DDT, this dipole moment is oriented from the surface into the solution.[38] Consequently, there is a net positively charged layer inside the solution, bound to the surface of the Au, held at V_{GS} by the power supply, which increases the electric field resulting from the applied gate voltage ($V_{GS} > 0$). Therefore, gating is enhanced and the TC is shifted toward lower values of V_{GS}, as observed in Figure 2, Stage 1 (DDT).

Stage 2, functionalization of the graphene with PBSE, results in a shift of $\Delta V_{Dirac} = +40 \pm 10$ mV (Figure 2, blue line). The

DOI: 10.1021/acssensors.8b00344
ACS Sens. 2019, 4, 286−293

functionalization of carbon surfaces with 1-pyrenebutyric acid leads to small shifts in chemical potential, actually smaller than those predicted by molecular dynamics simulations,[39] due to more effective screening by water molecules, which can more readily penetrate between the carboxylic acid group, an ester group in the case of PBSE, and the carbon surface. The large shift observed in the TC after this step (Figure 2, stage 2) is likely due to the surface effects, as confirmed by Raman spectroscopy results (cf. Figure S4 and related discussion in the SI). The sign of the TC shift, toward more positive V_{GS}, indicates that there is additional p-doping of the graphene upon $\pi-\pi$ stacking of the linker.

The last two functionalization stages are the immobilization of the DNA probes (stage 3) followed by the passivation of the channel with ethanolamine (ETA) (stage 4). Stage 4 is necessary to minimize nonspecific reactions. After stage 3, there will be many unreacted NHS-ester ligands that will be blocked by reacting with ETA. After immobilization of the single-stranded DNA (ssDNA) probes via PBSE linkers, there is a large shift of $\Delta V_{Dirac} \approx -70$ mV between stages 3 and 2. When ETA blocks the unreacted NHS-ester ligands of PBSE, the difference in V_{Dirac} between stages 4 and 2 is reduced to $\Delta V_{Dirac} \approx -50$ mV. This decrease of ΔV_{Dirac} is likely explained by removal of weakly bound DNA strands from the surface after incubation in the ETA solution (Figure 2, pink and green lines respectively).

The Surface Density of Probe DNA. The density of probe DNA immobilized on the surface of a biosensor will set its dynamic range, and may significantly influence its behavior.[36,37,40,41] We have used two independent techniques to investigate the surface density of DNA probes achievable on our devices.

Quartz crystal microbalance (QCM) enables in situ gravimetric measurements of surface adsorption in solution, with sensitivity sufficient to detect full or partial layers of biomolecules and biorecognition events.[42] With solution parameters adjusted to be compatible with QCM measurements (as described in the SI), we have measured the surface density of DNA probes immobilized on graphene via PBSE to be $1.0 \pm 0.1 \times 10^{13}$ cm^{-2}. In all the control experiments, nonspecific adsorption of DNA produced at least 50% lower surface density, in agreement with previous results for DNA immobilization on gold.[37]

X-ray photoelectron spectroscopy (XPS) was used as an ex situ technique complementary to QCM, extending the methodology previously developed for quantification of molecular layers on surfaces.[37,43−45] The presence of the NHS-ester ligands of PBSE was confirmed by observing the characteristic[46] N 1s component at 401.6 eV (Figure S5). After DNA immobilization, this NHS-ester N 1s component is replaced by one at 400.8 eV, matching the position expected for the thymine homo-oligonucleotides[37,43] that we used as simulated probes. Furthermore, the N 1s shoulder at ca. 399.3 eV is consistent with a fraction of the probes being in contact with the substrate.[43] The surface density of probes calculated based on the XPS data is $1.5 \pm 0.2 \times 10^{13}$ cm^{-2}, in agreement with QCM results and with values previously reported for high-quality DNA-functionalized biosensor surfaces.[36,37,43]

DNA Biosensor Performance. After the last passivation step (ETA, step 4, Figure S1), the device is ready to detect the target DNA. For each target concentration, a droplet of the solution containing the target was placed on the transistor channel and allowed to interact with the probe DNA for a fixed time interval of 40 min, to allow the hybridization to be accomplished. After this time a stringency rinse using the measuring buffer (10 mM PB, pH 7.4) was performed in order to remove strands that did not hybridize or were weakly bound, and finally the transistor TCs were measured.

Figure 3A shows the EGFET TCs for different concentrations of fully complementary DNA ($cDNA_{PM}$) target. As the

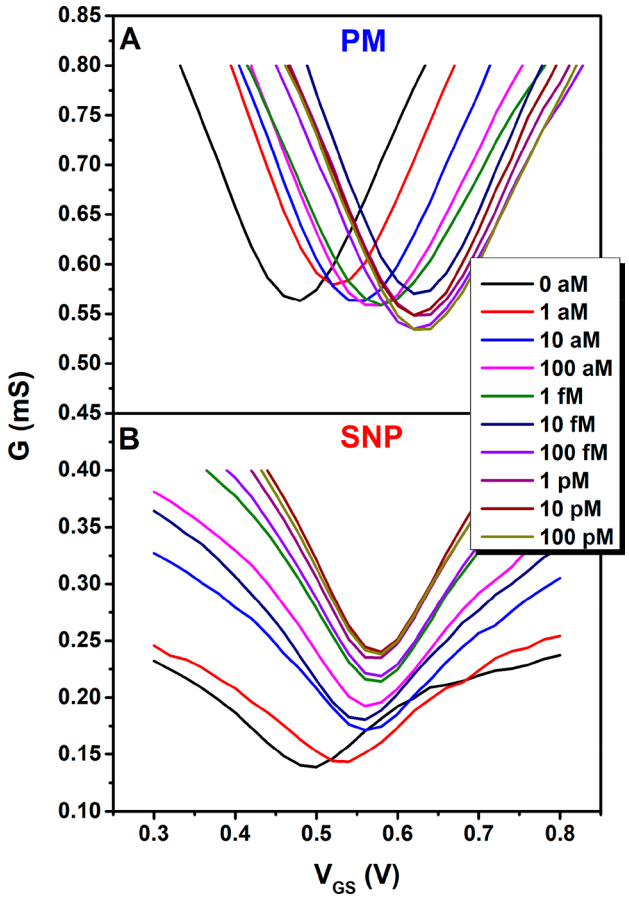

Figure 3. Characteristic transfer curves for (A) perfect match (PM) complementary DNA and (B) SNP containing cDNA, for the different concentrations studied.

concentration of $cDNA_{PM}$ increases, in a range between 1 aM and 100 fM, a progressive shift in V_{Dirac} toward more positive V_{GS} is observed. For $[cDNA_{PM}] > 100$ fM, V_{Dirac} does not move any more, reaching saturation. The trajectory of V_{Dirac} as a function of $[cDNA_{PM}]$ is clearly visible in Figures 4 and S6A where V_{Dirac} is plotted as a function of $[cDNA_{PM}]$. The isoelectric point of DNA is close to 5.0,[47] therefore, at physiological pH, DNA molecules are negatively charged. The electrostatic field of these charges immobilized near the graphene surface will induce, by local gating, p-doping, which shifts V_{Dirac} to more positive V_{GS}.[22] Saturation at 100 fM indicates reaching an equilibrium between hybridization and electrostatic repulsion between DNA probes and targets.

In the dynamic range of the biosensor, a sensitivity of 24 mV/decade is achieved, which is an improvement of 7 mV/decade when compared to the best results reported in the literature.[19] In the case of SNP-containing cDNA, the shift of V_{Dirac} with increasing concentrations of cDNA (Figures 3B and 4, red circles) is apparent only as a weak trend, visible upon fitting the entire set of data to a straight line. This behavior is

DOI: 10.1021/acssensors.8b00344
ACS Sens. 2019, 4, 286−293

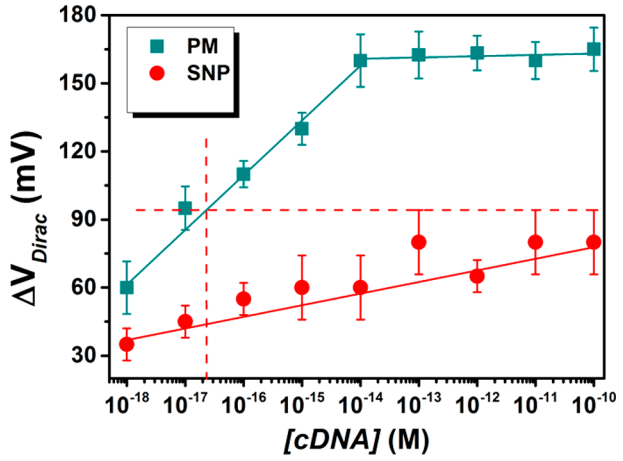

Figure 4. Calibration curves for the bio-FET sensor. Green squares refer to target DNA fully complementary to the probe and red circles to SNP target. The error bars are standard deviations of measurement with five different devices.

expected since the DNA duplex can still be formed between the probe DNA and the SNP-containing cDNA, but it is unstable and most of the duplexes formed are probably unzipped during the stringency rinse.[23] As a control experiment, a probe DNA fully complementary to the SNP-containing target was immobilized on the graphene FET channel and an experiment, conducted in the same manner as before, showed that the sensor could indeed detect the perfectly matching sequence (Figure S6c).

It is important to note that after the probe immobilization in stage 3, ΔV_{Dirac} was negative, whereas upon probe hybridization with target DNA all ΔV_{Dirac} shifts are positive. Table 1 summarizes published data reporting ΔV_{Dirac} shifts observed in liquid-gate bio-FETs based on graphene, or graphene-related materials. With no exception,[20,21,46] upon DNA hybridization, devices that use no linker have $\Delta V_{Dirac} < 0$, while devices using PBSE linkers,[25,47] including ours, have $\Delta V_{Dirac} > 0$. A simple interpretation for the left-shift of V_{Dirac} when no linker is used is duplex DNA desorption from the graphene surface upon probe-target hybridization. This will leave a lower concentration of negatively charged pDNA for local gating on the graphene surface and consequently V_{Dirac} undergoes a negative shift (graphene becomes less p-doped).[48] The positive shift upon DNA hybridization observed with PBSE linkers has been discussed above and is a consequence of forming the duplex tethered to the graphene surface via the PBSE linker. These tethered DNA hybrids will not desorb, except for a small fraction of hybrids formed with pDNA directly adsorbed to graphene.

In contrast, the initial immobilization of pDNA on the graphene surface via PBSE has the same effect as that of an electron-donating group ($\Delta V_{Dirac} < 0$). Literature reports on doping single-layer graphene with π-stacked aromatic molecules (e.g., refs 49,50), show that *p*-doping is observed when stacking is with electron-withdrawing groups, and *n*-doping occurs when stacking with electron-donating groups. Because the pDNA single strands are flexible, they can partially interact with the graphene surface via $\pi-\pi$ stacking of the nucleobase aromatic rings (pyrimidines and purines), as indicated by the N 1s shoulder at ca. 399.3 eV in XPS data (Figure S5).[43]

However, upon DNA hybridization, the much stiffer duplex DNA attached covalently to the PBSE linker will extend away from the surface, overcoming the $\pi-\pi$ interaction of pDNA with the surface. The mechanism of interaction of these upright hybrids with graphene is now exclusively by local gating via modulation of the EDL capacitance, as discussed above.

Figure 4 shows the sensor output data for the two series of measurements, with perfectly matched (squares) and SNP-containing (circles) targets. The sensor exhibits, for the perfectly matched target, a linear range between 1 aM and 10 fM before saturating at 100 fM. We use the maximum signal from the SNP-containing target in Figure 4, to set the limit of detection (LoD) of the sensor to ≈25 aM, as indicated by the dashed lines in Figure 4.

Each data point in Figure 4 is an average of five measurements independently made with five different transistors and the error bars are one standard deviation. These results compare favorably to the recently reported device (Xu et al.[51] in Table 1), which exhibited the same linear dynamic range: four decades of DNA concentration. In the studies summarized in Table 1, lowering the LoD had been attributed primarily to the material of the FET channel, e.g., moving from few-layer graphene to SLG[21] or from transferred to directly grown CVD graphene.[51] The practical difficulties of reaching LoD < 1 nM have been noted in previous experimental[25] and theoretical[52] studies, as longer measurement times are required for a sufficient number of DNA targets to reach the sensor surface. The rationale for our optimization strategy was to increase the probability that the rare target arrival events to the sensor surface will encounter a probe and become successfully captured, via increasing the surface density of the probes and the ionic strength of the hybridization

Table 1. Literature Survey of Graphene-Based Electrolyte-Gated FET DNA Biosensor Characteristics

			FET channel					
work	LoD (M)[a]	hybridization conditions	growth/transfer	$L \times W$ (μm^2)	linker	gate	shift in V_{Dirac}[b]	fabrication
Chen et al.[21]	1×10^{-12}	1× PBS[c]	CVD on Cu/PMMA	$10^4 \times 10^4$	none	Ag-wire	negative	contacts w/Ag paste
Dong et al.[20]	1×10^{-11}	PB1, pH 7.4[d]	CVD on Ni/PMMA	3000 × 10000	none	Ag-wire	negative	contacts w/Ag-paint
Xu et al.[25]	1×10^{-11}	0.01× PBS, pH 7.8	CVD on Cu/PMMA	45 × 90	PBSE	Pt-wire	positive	μ-fluidic platform, optical litho.
Xu et al.[51]	1×10^{-13}	0.01× PBS, pH 7.4	CVD on sapphire/ direct growth	43 × 90	PBSE	Ag/AgCl wire	positive	μ-fluidic platform, optical litho.
this work	1×10^{-17}	PB2, pH 7[e]	CVD on Cu/PMMA	25 × 75	PBSE	Au-planar, integrated	positive	planar, optical litho., contacts prepatterned

[a]In synthetic medium. [b]Upon DNA hybridization. [c]137 mM NaCl, 2.7 mM KCl, 4.3 mM Na_2HPO_4, 1.47 mM KH_2PO_4. [d]10 mM PB, 250 mM NaCl. [e]10 mM PB, 150 mM NaCl, 50 mM $MgCl_2$.

DOI: 10.1021/acssensors.8b00344
ACS Sens. 2019, 4, 286−293

solution, given the well-known importance of these parameters.[36,37,40,43] The LoD achieved in our work clearly indicates that using transferred CVD-graphene as the channel material does not intrinsically limit the sensitivity of bio-FETs. Of course, in practical devices lowering the LoD results in shifting the dynamic range to lower DNA concentrations, e.g., the entire dynamic range demonstrated for the device in ref 51 is within the saturation range of ours (Figure 4). Accordingly, bio-FET device optimization needs to be application-specific, to appropriately inform the choices of the design parameters.[36,37]

CONCLUSIONS

A bio-FET based on transferred CVD-graphene was successfully developed for the detection of DNA hybridization. The probe DNA molecules were immobilized on the graphene surface via NHS reaction with PBSE, a heterobifunctional linker. The unreacted NHS ligands of PBSE are then blocked by incubation with ethanolamine, to reduce nonspecific interactions during the subsequent measurements. The results show that the graphene bio-FET can detect target DNA molecules down to attomolar levels with a sensitivity of 24 mV/decade, with a dynamic range of 10^4.

This label-free graphene bio-FET has great potential, particularly for applications where the levels of mutated DNA are much higher than those of normal DNA, due to the ability to detect full hybridization down to 25 aM, compared to 5 orders of magnitude higher levels of SNP-containing targets. Further studies need to be performed in order to evaluate the performance of the bio-FET in the presence of interferents and complex matrices.

ASSOCIATED CONTENT

Supporting Information

The Supporting Information is available free of charge on the ACS Publications website at DOI: 10.1021/acssensors.8b00344.

Schematic representation of biosensor development, complete TC sets for all the stages and different concentrations, Raman spectra of the various stages, XPS results, SEM images of the FET, non-normalized calibration curves, and electrochemical measurements including the experimental details (PDF)

AUTHOR INFORMATION

Corresponding Author

*E-mail: pedro.alpuim.us@inl.int.

ORCID

Dmitri Y. Petrovykh: 0000-0001-9089-4076

Pedro Alpuim: 0000-0001-9875-6188

Present Address

[‖]R.C.: AXES Research Group, Chemistry Department, Groenenborgerlaan 171, 2020 Antwerp, Belgium.

Author Contributions

Experiments were designed by R.C., J.B., and P.A. Fabrication of EGFETs and testing was performed by G.M.Jr., J.B., and R.C. Graphene growth and transfer was performed by G.M.Jr. Graphene characterization was performed by M.F.C. XPS and QCM measurements were performed by J.R.G. and D.Y.P. The manuscript and figures were prepared by R.C., J.B., M.F.C., J.R.G., D.Y.P, and P.A. P.A. supervised all aspects of this work. The manuscript was written through contributions of all authors. All authors have given approval to the final version of the manuscript.

Notes

The authors declare no competing financial interest.

ACKNOWLEDGMENTS

This work was partially supported by the Portuguese Foundation for Science and Technology (FCT) in the framework of the Strategic Funding UID/FIS/04650/2013 and Project POCI-01-0145-FEDER-031069 (PORTGRAPHE). G.M.Jr. acknowledges a PhD grant (no. 237630/2012-5) from CNPq−Brazil. J.B. and D.Y.P. acknowledge European funding from FROnTHERA project under contract NORTE-01-0145-FEDER-000023.

REFERENCES

(1) Janasek, D.; Franzke, J.; Manz, A. Scaling and the Design of Miniaturized Chemical-Analysis Systems. *Nature* **2006**, *442* (7101), 374−380.

(2) Barany, F. Genetic Disease Detection and DNA Amplification Using Cloned Thermostable Ligase. *Proc. Natl. Acad. Sci. U. S. A.* **1991**, *88* (1), 189−193.

(3) Shapiro, J. A. Genome Informatics: The Role of DNA in Cellular Computations. *Biol. Theory* **2006**, *1* (3), 288−301.

(4) Jin, L.; Chakraborty, R. Population Structure, Stepwise Mutations, Heterozygote Deficiency and Their Implications in DNA Forensics. *Heredity* **1995**, *74* (3), 274−285.

(5) Du, Y.; Guo, S.; Dong, S.; Wang, E. An Integrated Sensing System for Detection of DNA Using New Parallel-Motif DNA Triplex System and Graphene-Mesoporous Silica-Gold Nanoparticle Hybrids. *Biomaterials* **2011**, *32* (33), 8584−8592.

(6) Mullis, K.; Faloona, F.; Scharf, S.; Saiki, R.; Horn, G.; Erlich, H. Specific Enzymatic Amplification of DNA in Vitro: The Polymerase Chain Reaction. *Cold Spring Harbor Symp. Quant. Biol.* **1986**, *51*, 263−273.

(7) Aleksić, M. M.; Kapetanović, V. An Overview of the Optical and Electrochemical Methods for Detection of DNA-Drug Interactions. *Acta Chim. Slov.* **2014**, 555−573.

(8) Drummond, T. G.; Hill, M. G.; Barton, J. K. Electrochemical DNA Sensors. *Nat. Biotechnol.* **2003**, *21* (10), 1192−1199.

(9) Park, H.-Y.; Dugasani, S. R.; Kang, D.-H.; Yoo, G.; Kim, J.; Gnapareddy, B.; Jeon, J.; Kim, M.; Song, Y. J.; Lee, S.; et al. M-DNA/Transition Metal Dichalcogenide Hybrid Structure-Based Bio-FET Sensor with Ultra-High Sensitivity. *Sci. Rep.* **2016**, *6*, 35733.

(10) Sze, S. M.; Ng, K. K. Physics and Properties of Semiconductors—A Review. In *Physics of Semiconductor Devices*; John Wiley & Sons, Inc., 2006; pp 5−75 DOI: 10.1002/9780470068328.ch1.

(11) Veigas, B.; Fortunato, E.; Baptista, P. Field Effect Sensors for Nucleic Acid Detection: Recent Advances and Future Perspectives. *Sensors* **2015**, *15* (5), 10380−10398.

(12) Justino, C. I. L.; Gomes, A. R.; Freitas, A. C.; Duarte, A. C.; Rocha-Santos, T. A. P. Graphene Based Sensors and Biosensors. *Trends Anal. Chem.* **2017**, *91*, 53−66.

(13) Bockris, J. O.; Devanathan, M. A. V.; Muller, K. On the Structure of Charged Interfaces. *Proc. R. Soc. A Math. Phys. Eng. Sci.* **1963**, *274* (1356), 55−79.

(14) Cui, Y.; Wei, Q.; Park, H.; Lieber, C. M. Nanowire Nanosensors for Highly Sensitive and Selective Detection of Biological and Chemical Species. *Science* **2001**, *293* (5533), 1289−1292.

(15) Yang, W.; Ratinac, K. R.; Ringer, S. R.; Thordarson, P.; Gooding, J. J.; Braet, F. Carbon Nanomaterials in Biosensors: Should You Use Nanotubes or Graphene. *Angew. Chem., Int. Ed.* **2010**, *49*, 2114−2138.

DOI: 10.1021/acssensors.8b00344
ACS Sens. 2019, 4, 286−293

(16) Lee, J.; Dak, P.; Lee, Y.; Park, H.; Choi, W.; Alam, M. A.; Kim, S. Two-Dimensional Layered MoS_2 Biosensors Enable Highly Sensitive Detection of Biomolecules. *Sci. Rep.* **2015**, *4*, 7352.
(17) Ohno, Y.; Maehashi, K.; Yamashiro, Y.; Matsumoto, K. Electrolyte-Gated Graphene Field-Effect Transistors for Detecting pH and Protein Adsorption. *Nano Lett.* **2009**, *9* (9), 3318−3322.
(18) Ohno, Y.; Maehashi, K.; Matsumoto, K. Label-Free Biosensors Based on Aptamer-Modified Graphene Field-Effect Transistors. *J. Am. Chem. Soc.* **2010**, *132* (51), 18012−18013.
(19) Lee, D.-W.; Lee, J.; Sohn, I. Y.; Kim, B.-Y.; Son, Y. M.; Bark, H.; Jung, J.; Choi, M.; Kim, T. H.; Lee, C.; et al. Field-Effect Transistor with a Chemically Synthesized MoS_2 Sensing Channel for Label-Free and Highly Sensitive Electrical Detection of DNA Hybridization. *Nano Res.* **2015**, *8* (7), 2340−2350.
(20) Dong, X.; Shi, Y.; Huang, W.; Chen, P.; Li, L.-J. Electrical Detection of DNA Hybridization with Single-Base Specificity Using Transistors Based on CVD-Grown Graphene Sheets. *Adv. Mater.* **2010**, *22* (14), 1649−1653.
(21) Chen, T.-Y.; Loan, P. T. K.; Hsu, C.-L.; Lee, Y.-H.; Tse-Wei Wang, J.; Wei, K.-H.; Lin, C.-T.; Li, L.-J. Label-Free Detection of DNA Hybridization Using Transistors Based on CVD Grown Graphene. *Biosens. Bioelectron.* **2013**, *41*, 103−109.
(22) Lin, C.-T.; Loan, P. T. K.; Chen, T.-Y.; Liu, K.-K.; Chen, C.-H.; Wei, K.-H.; Li, L.-J. Label-Free Electrical Detection of DNA Hybridization on Graphene Using Hall Effect Measurements: Revisiting the Sensing Mechanism. *Adv. Funct. Mater.* **2013**, *23* (18), 2301−2307.
(23) Zheng, C.; Huang, L.; Zhang, H.; Sun, Z.; Zhang, Z.; Zhang, G.-J. Fabrication of Ultrasensitive Field-Effect Transistor DNA Biosensors by a Directional Transfer Technique Based on CVD-Grown Graphene. *ACS Appl. Mater. Interfaces* **2015**, *7* (31), 16953−16959.
(24) Cai, B.; Wang, S.; Huang, L.; Ning, Y.; Zhang, Z.; Zhang, G.-J. Ultrasensitive Label-Free Detection of PNA−DNA Hybridization by Reduced Graphene Oxide Field-Effect Transistor Biosensor. *ACS Nano* **2014**, *8* (3), 2632−2638.
(25) Xu, S.; Zhan, J.; Man, B.; Jiang, S.; Yue, W.; Gao, S.; Guo, C.; Liu, H.; Li, Z.; Wang, J.; et al. Real-Time Reliable Determination of Binding Kinetics of DNA Hybridization Using a Multi-Channel Graphene Biosensor. *Nat. Commun.* **2017**, *8*, 14902.
(26) Ohno, Y.; Okamoto, S.; Maehashi, K.; Matsumoto, K. Direct Electrical Detection of DNA Hybridization Based on Electrolyte-Gated Graphene Field-Effect Transistor. *Jpn. J. Appl. Phys.* **2013**, *52*, 110107.
(27) Xu, G.; Abbott, J.; Qin, L.; Yeung, K. Y. M.; Song, Y.; Yoon, H.; Kong, J.; Ham, D. Electrophoretic and Field-Effect Graphene for All-Electrical DNA Array Technology. *Nat. Commun.* **2014**, *5*, 4866.
(28) Hybridization of two different strands of DNA or RNA. mfold.rit.albany.edu; http://unafold.rna.albany.edu/?q=DINAMelt/Hybrid2.
(29) Campos, R.; Machado, G.; Cerqueira, M. F.; Borme, J.; Alpuim, P. Wafer Scale Fabrication of Graphene Microelectrode Arrays for the Detection of DNA Hybridization. *Microelectron. Eng.* **2018**, *189*, 85−90.
(30) Vieira, N. C. S.; Borme, J.; Machado, G.; Cerqueira, F.; Freitas, P. P.; Zucolotto, V.; Peres, N. M. R.; Alpuim, P. Graphene Field-Effect Transistor Array with Integrated Electrolytic Gates Scaled to 200 mm. *J. Phys.: Condens. Matter* **2016**, *28* (8), 085302.
(31) Aguiar, F. A.; Campos, R.; Wang, C.; Jitchati, R.; Batsanov, A. S.; Bryce, M. R.; Kataky, R. Comparative Electrochemical and Impedance Studies of Self-Assembled Rigid-Rod Molecular Wires and Alkanethiols on Gold Substrates. *Phys. Chem. Chem. Phys.* **2010**, *12* (44), 14804−14811.
(32) Chen, R. J.; Zhang, Y.; Wang, D.; Dai, H. Noncovalent Sidewall Functionalization of Single-Walled Carbon Nanotubes for Protein Immobilization. *J. Am. Chem. Soc.* **2001**, *123* (16), 3838−3839.
(33) Tlili, C.; Cella, L. N.; Myung, N. V.; Shetty, V.; Mulchandani, A. Single-Walled Carbon Nanotube Chemoresistive Label-Free Immunosensor for Salivary Stress Biomarkers. *Analyst* **2010**, *135* (10), 2637−2642.
(34) Mayorov, A. S.; Elias, D. C.; Mukhin, I. S.; Morozov, S. V.; Ponomarenko, L. A.; Novoselov, K. S.; Geim, A. K.; Gorbachev, R. V. How Close Can One Approach the Dirac Point in Graphene Experimentally? *Nano Lett.* **2012**, *12* (9), 4629−4634.
(35) Chen, J.-H.; Ishigami, M.; Jang, C.; Hines, D. R.; Fuhrer, M. S.; Williams, E. D. Printed Graphene Circuits. *Adv. Mater.* **2007**, *19* (21), 3623−3627.
(36) Gong, P.; Lee, C.-Y.; Gamble, L. J.; Castner, D. G.; Grainger, D. W. Hybridization Behavior of Mixed DNA/Alkylthiol Monolayers on Gold: Characterization by Surface Plasmon Resonance and ^{32}P Radiometric Assay. *Anal. Chem.* **2006**, *78*, 3326−3334.
(37) Schreiner, S. M.; Shudy, D. F.; Hatch, A. L.; Opdahl, A.; Whitman, L. J.; Petrovykh, D. Y. Controlled and Efficient Hybridization Achieved with DNA Probes Immobilized Solely through Preferential DNA-Substrate Interactions. *Anal. Chem.* **2010**, *82* (7), 2803−2810.
(38) Alloway, D. M.; Hofmann, M.; Smith, D. L.; Gruhn, N. E.; Graham, A. L.; Colorado, R.; Wysocki, V. H.; Lee, T. R.; Lee, P. a.; Armstrong, N. R. Interface Dipoles Arising from Self-Assembled Monolayers on Gold: UV-Photoemission Studies of Alkanethiols and Partially Fluorinated Alkanethiols. *J. Phys. Chem. B* **2003**, *107* (42), 11690−11699.
(39) Lerner, M. B.; Resczenski, J. M.; Amin, A.; Johnson, R. R.; Goldsmith, J. I.; Johnson, A. T. C. Toward Quantifying the Electrostatic Transduction Mechanism in Carbon Nanotube Molecular Sensors. *J. Am. Chem. Soc.* **2012**, *134* (35), 14318−14321.
(40) Campos, R.; Ferapontova, E. E. Electrochemistry of Weakly Adsorbed Species: Voltammetric Analysis of Electron Transfer between Gold Electrodes and Ru Hexaamine Electrostatically Interacting with DNA Duplexes. *Electrochim. Acta* **2014**, *126*, 151−157.
(41) Álvarez-Martos, I.; Campos, R.; Ferapontova, E. E. Surface State of the Dopamine RNA Aptamer Affects Specific Recognition and Binding of Dopamine by the Aptamer-Modified Electrodes. *Analyst* **2015**, *140* (12), 4089−4096.
(42) Ray, S.; Steven, R. T.; Green, F. M.; Höök, F.; Taskinen, B.; Hytönen, V. P.; Shard, A. G. Neutralized Chimeric Avidin Binding at a Reference Biosensor Surface. *Langmuir* **2015**, *31* (6), 1921−1930.
(43) Petrovykh, D. Y.; Kimura-Suda, H.; Tarlov, M. J.; Whitman, L. J. Quantitative Characterization of DNA Films by X-Ray Photoelectron Spectroscopy. *Langmuir* **2004**, *20* (2), 429−440.
(44) Petrovykh, D. Y.; Kimura-Suda, H.; Opdahl, A.; Richter, L. J.; Tarlov, M. J.; Whitman, L. J. Alkanethiols on Platinum: Multicomponent Self-Assembled Monolayers. *Langmuir* **2006**, *22* (6), 2578−2587.
(45) Fears, K. P.; Clark, T. D.; Petrovykh, D. Y. Residue-Dependent Adsorption of Model Oligopeptides on Gold. *J. Am. Chem. Soc.* **2013**, *135* (40), 15040−15052.
(46) Lim, C. Y.; Owens, N. A.; Wampler, R. D.; Ying, Y.; Granger, J. H.; Porter, M. D.; Takahashi, M.; Shimazu, K. Succinimidyl Ester Surface Chemistry: Implications of the Competition between Aminolysis and Hydrolysis on Covalent Protein Immobilization. *Langmuir* **2014**, *30* (43), 12868−12878.
(47) Sherbet, G. V.; Lakshmi, M. S.; Cajone, F. Isoelectric Characteristics and the Secondary Structure of Some Nucleic Acids. *Biophys. Struct. Mech.* **1983**, *10* (3), 121−128.
(48) Yin, Z.; He, Q.; Huang, X.; Zhang, J.; Wu, S.; Chen, P.; Lu, G.; Chen, P.; Zhang, Q.; Yan, Q.; et al. Real-Time DNA Detection Using Pt Nanoparticle-Decorated Reduced Graphene Oxide Field-Effect Transistors. *Nanoscale* **2012**, *4* (1), 293−297.
(49) Dong, X.; Fu, D.; Fang, W.; Shi, Y.; Chen, P.; Li, L.-J. Doping Single-Layer Graphene with Aromatic Molecules. *Small* **2009**, *5* (12), 1422−1426.
(50) Zhang, Z.; Huang, H.; Yang, X.; Zang, L. Tailoring Electronic Properties of Graphene by $\pi-\pi$ Stacking with Aromatic Molecules. *J. Phys. Chem. Lett.* **2011**, *2* (22), 2897−2905.

DOI: 10.1021/acssensors.8b00344
ACS Sens. 2019, 4, 286−293

(51) Xu, S.; Jiang, S.; Zhang, C.; Yue, W.; Zou, Y.; Wang, G.; Liu, H.; Zhang, X.; Li, M.; Zhu, Z.; et al. Ultrasensitive Label-Free Detection of DNA Hybridization by Sapphire-Based Graphene Field-Effect Transistor Biosensor. *Appl. Surf. Sci.* **2018**, *427*, 1114−1119.
(52) Sheehan, P. E.; Whitman, L. J. Detection Limits for Nanoscale Biosensors. *Nano Lett.* **2005**, *5*, 803.

DOI: 10.1021/acssensors.8b00344
ACS Sens. 2019, 4, 286−293

Supporting Information

Attomolar label-free detection of DNA hybridization with electrolyte-gated graphene field-effect transistors

Rui Campos[†,ζ], Jérôme Borme[†], Joana Rafaela Guerreiro[†], George Machado, Jr.[†,#], Maria Fátima Cerqueira[†,#], Dmitri Y Petrovykh[‡], and Pedro Alpuim[†,#,*]

[†] Department of Quantum and Energy Materials, International Iberian Nanotechnology Laboratory, 4715-330, Braga, Portugal

[‡] Department of Life Sciences, International Iberian Nanotechnology Laboratory, 4715-330, Braga, Portugal

[#] Center of Physics, University of Minho, 4710-057, Braga, Portugal

MATERIALS AND METHODS

Graphene transfer A layer of PMMA 950k (AR-P 679.04, Allresist, Germany) is spin-coated on top of the top side of the copper covered in graphene. The layer of graphene on the bottom side is removed by oxygen plasma. The copper is dissolved in iron chloride 0.5 M at 35 °C. The floating graphene and its temporary PMMA substrate are cleaned in a solution of hydrochloric acid 2 % for 30 min and rinsed into de-ionised water (resistivity ≥ 18 MΩ) for 5 minutes. The cleaning and rinsing procedures are repeated five times. Graphene is then transferred onto the pre-patterned substrate. In order to improve the removal of water between the wafer and graphene, the wafer is first submitted to a hydrophobic priming using vapor HDMS. The transferred graphene is dried in oven at 180 °C for 12 hours. After cooling down, the wafer is placed in an acetone bath for 2 hours to remove PMMA.

Electrochemical Measurements Capacitance measurements were performed using a Autolab 302N potentiostat running NOVA 2.1 software. The working electrode was a microelectrode array with 60 microelectrodes of 40 μm diameter and a distance between microelectrodes of 400 μm in a hexagonal arrangement. The reference and counter electrodes were, respectively, Ag/AgCl 3 M KCl from metrohm and a platinum flag of 1 cm^2. The electrochemical area determination was performed in a chip to which graphene had not been transferred, cyclic voltammetry was performed in 0.1 M H_2SO_4. The capacitance was determined from electrochemical impedance spectroscopy measurements performed in PB 10 mM, in a range of potentials between -0.5 V and

0.5 V *vs.* Ag/AgCl with 50 mV intervals with each measurement being performed in a range of frequencies (100 kHz to 1Hz, amplitude 5 mV).

Raman Characterization. The EGFET channel has been characterized/monitored after each functionalization step by Confocal Raman spectroscopy measurements, performed at room temperature in a back scattering geometry, on a WITec Alpha300 R confocal Raman microscope using a 532 nm Nd:YAG laser for excitation, at an output power of 1.5 mW, and an objective ×50 lens (Zeiss, NA=0.7). The spectra were collected with a 600 groove/mm grating using 5 acquisitions with 2 s acquisition time. After stage 2 of the functionalization process (PBSE immobilization), a 633 nm excitation line from a He-Ne laser was also used. After each step multiple Raman measurements were performed in different points of the channel to confirm that the spectra acquired were representative.

Biosensor Development.

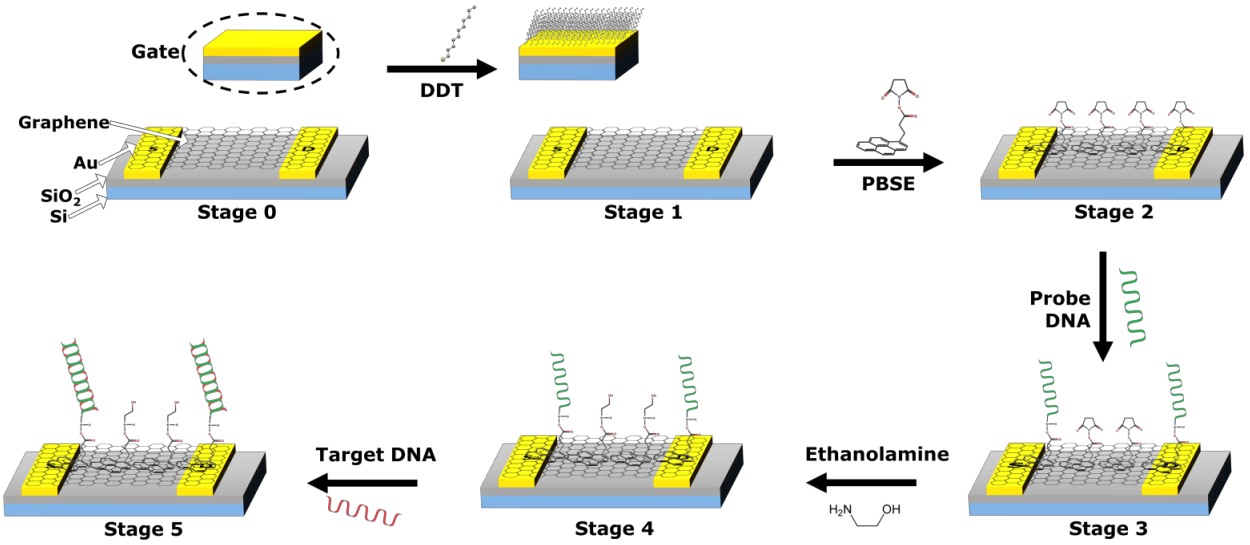

Figure S1. Schematic view of the stages of the biosensor development: Stage 0: as-fabricated graphene transistor; Stage 1: DDT gate passivation; Stage 2: immobilization of the linker (PBSE); Stage 3: functionalization with probe DNA; Stage 4: blocking with ethanolamine; Stage 5: biorecognition.

QCM-D experiments. Quartz crystal microbalance with dissipation (QCM-D) was used for *in situ* characterization of the immobilization of DNA probes and of the subsequent DNA hybridization on model graphene surfaces prepared following protocols similar to those used for the EGFET device.

The QCM measurements were performed in a QSense E1 system (Biolin Scientific). AT-cut quartz crystals having gold electrodes of the working surface coated with ca. 50 nm of silicon

oxide (QSX 335, Biolin Scientific) were used as substrates for single-layer graphene transfer. QCM measurements for the fundamental (ca. 4.95 MHz) frequency and at its 6 odd overtones (n = 3, 5, 7, 9, 11, 13) were carried out under a flow rate of ca. 0.075 ml/min at a constant temperature of 20 °C (set within <1 °C from RT, at which the solutions have been stabilized prior to the measurements). The measurements produced consistent results in experiments on two different QCM crystals.

A QCM sensor with silicon oxide surface first was cleaned in a 1% Alconox solution at 60 ºC for 1 h followed by rinsing in deionized water and isopropanol. After cleaning the sensor in oxygen plasma, graphene was transferred onto the sensor surface following a procedure analogous to that used for EGFETs. Prior to QCM-D measurements, the graphene surface was modified with PBSE heterobifunctional linker (10 mM in DMF for 2 h) and then placed inside the QCM-D chamber.

After achieving a stable baseline with the running buffer 0.99 M $CaCl_2$-TE (1× TE buffer is 10 mM Tris·HCl and 1 mM EDTA) at a flow rate of 0.075 ml/min, 1 ml of the 25-nt DNA probe solution (1 μM in 0.99 M $CaCl_2$-TE) was recirculated through the chamber and allowed to react for ca. 30 min followed by a rinse in the blank running buffer to remove non-specifically bound DNA probes. Blocking the surface with ethanolamine (100 mM at pH 8 in water for 30 min) was performed outside the QCM chamber. After remounting the sensor in the chamber, a new baseline was collected and 1 mL of the DNA target (25-nt perfect match to the probe) solution (1 μM in 0.99 M $CaCl_2$-TE was recirculated through the chamber and allowed to react for ca. 30 min followed by a rinse in the blank running buffer to remove non-specifically bound DNA targets.

Specificity of the DNA probe immobilization and of the target recognition was evaluated in control experiments whereby: (1) the target (i.e., sequence of the same length and similar composition, but without the terminal amine modification) was used instead of the probe; (2) probe immobilization was attempted onto a surface after ethanolamine blocking; (3) the probe was used instead of the target, to simulate a non-complementary target sequence.

The surface density of DNA was estimated by using the Sauerbrey equation (Eq. 1):

$$\Delta m = -C \cdot \Delta f / n, \quad \text{(Eq. 1)}$$

where C is the mass sensitivity constant (C = 18.1 $ng \cdot cm^{-2} \cdot Hz^{-1}$ for the employed QCM sensors), n is the overtone number, Δm is the adsorbed mass per unit area ($ng \cdot cm^{-2}$), and Δf is the measured frequency shift (Hz).

XPS experiments. The chemical immobilization of the amine-modified simulated-probe DNA sequence (30-nt) was also investigated by x-ray photoelectron spectroscopy (XPS). Silicon surfaces with a thick silicon oxide layer were used as substrates, on which the graphene transfer and subsequent modification steps were carried out analogously to those on the QCM sensors described above. A simulated probe sequence, a 30-nt thymine homo-oligonucleotide (T_{30}), was used instead of the pDNA sequence to produce an XPS signature that is easier to interpret in terms of surface density and conformation of the surface-immobilized DNA strands.

Representative graphene surfaces before and after functionalization with PBSE and simulated-probe DNA were characterized in an ESCALAB 250 Xi system (Thermo Scientific) using a nonmonochromated Al Kα X-ray source, with an analyzer-defined analysis spot of <1 mm^2. Peak fitting was performed in Avantage instrument software (Thermo Scientific), choosing a minimal number of components that produced random residuals consistently for all the samples; a convolution of Gaussian and Lorentzian line shapes was used for all the spectral components. To avoid differential charging possible on the substrates with a thick layer of silicon oxide, uniform charge neutralization was provided by beams of low-energy (≤10 eV) Ar^+ ions and electrons guided by a magnetic lens; consistent charge neutralization was verified by observing the adventitious C 1s peak at 284.7±0.1 eV and the oxide substrate Si $2p_{3/2}$ peak at 103.7±0.1 eV for all samples. The position of the Si $2p_{3/2}$ component could be monitored because silicon oxide substrate in these measurements was of sufficient quality to exhibit the asymmetry due to the doublet structure, with FWHM of 1.5±0.1 eV for each of the spin-orbit components in the fits (Figure S5).

RESULTS

Transfer curve measurements

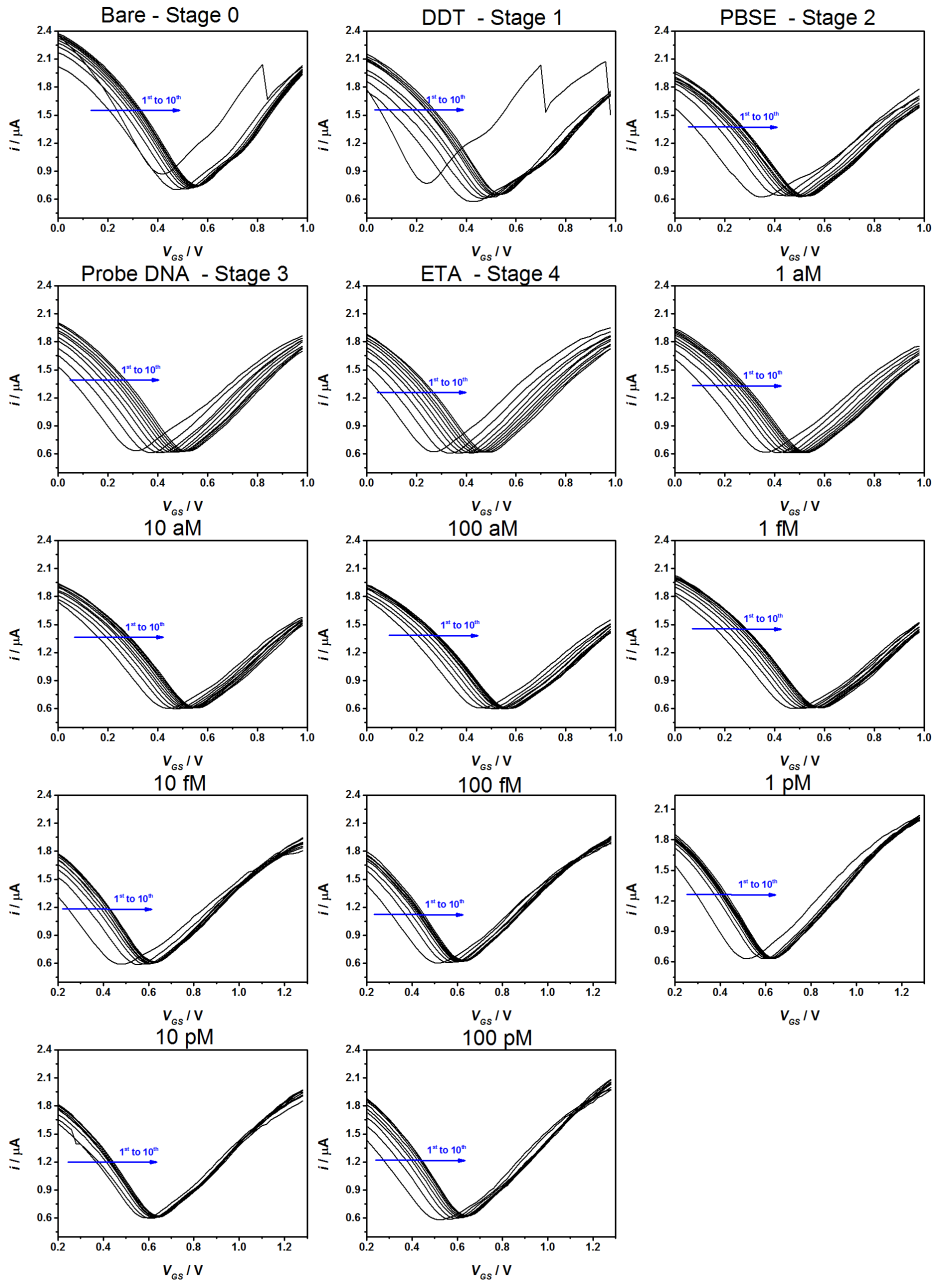

Figure S2 – Complete TC sets for all the stages and different concentrations.

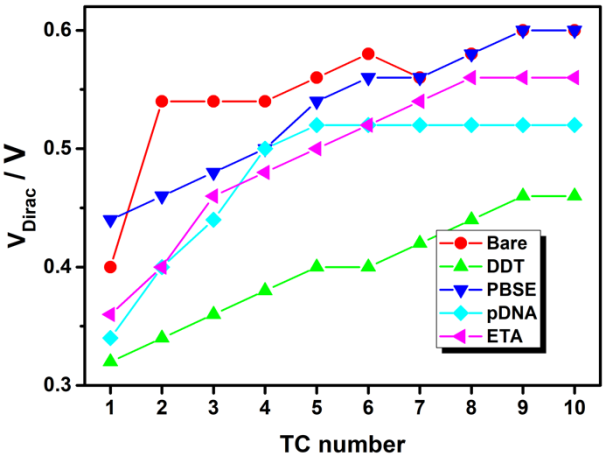

Figure S3. Position of V_{Dirac} as a function of the TC curve number. Curves are numbered sequentially in time.

Raman Characterization

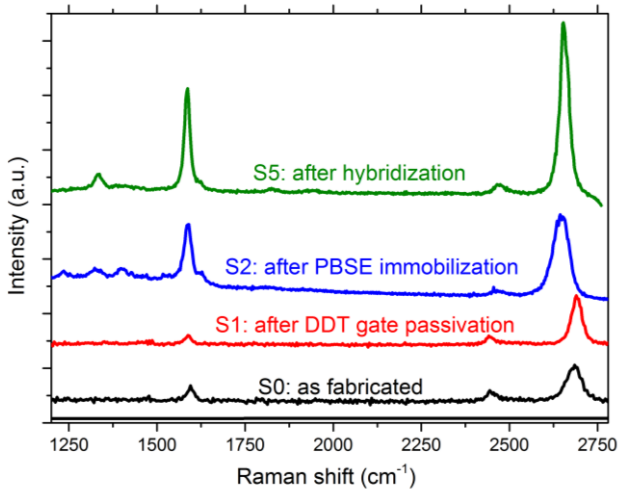

Figure S4 – Characteristic room temperature Raman spectra of the graphene channel of the transistor after stages 0, 1, 2, and 5 of the functionalization/biorecognition process. Spectra S0 and S1 were obtained with 532 nm laser excitation line and S2 and S5 with 633 nm laser line.

Carbon based materials have two distinctive features in their Raman spectra, namely the G mode at ≈ 1580 cm^{-1}, and the 2D mode at ≈ 2700 cm^{-1}. The G mode is the most intense mode in graphitic samples. The 2D mode is a two-phonon double resonance Raman mode and it is the most intense mode in single layer graphene. The 1st order D mode (≈1350 cm^{-1}) is absent in pristine graphene due to the Raman selection rules. If this mode is present, it means that graphene has defects, which breakdown the selection rules. The D intensity is proportional to

the sample defect level.[1,2] The Raman spectrum acquired after stage 0 (Figure S4, black line) shows that the CVD grown graphene is single layer (I2D/IG > 1) with almost no defects, as seen by the absence of the D mode. The passivation of the gate with DDT in stage 1 did not influence the graphene quality as can be seen in the Raman spectrum (Figure S4, red line) where the defect D mode is absent, and is overall a very similar spectrum to the one acquired after stage 0, with a FWHM of the 2D peak of 33 cm^{-1}. However, after the functionalization of the graphene channel with PBSE (stage 2) the Raman spectrum shows some extra features in the range 1200-1400 cm^{-1}. The spectrum has been fitted, using one Lorentzian function for each new contribution, and the fitting spectrum clearly shows two new peaks at ≈ 1235 cm^{-1} and ≈ 1398 cm^{-1}, and the appearance of the D mode. The new peaks are assigned to C-H bending and C=C in-plane vibration modes of the pyrene group, respectively,[3–5] which is part of the PBSE linker. These modes have a larger FWHM than found in pure pyrene. A broadening and a shift in pyrene Raman peak positions was reported in relation with surface effects.[5]

XPS characterization

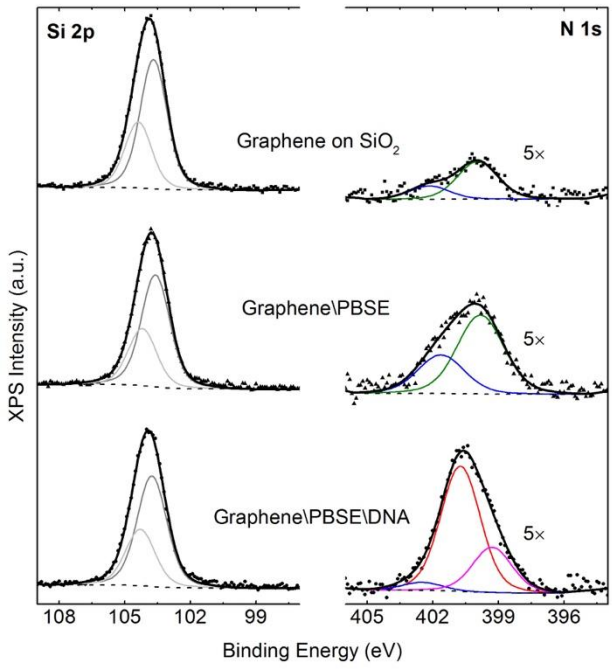

Figure S5 – XPS signatures acquired after individual steps in functionalization of graphene with DNA probes. The Si 2p (left) and N 1s (right, shown multiplied by a factor of 5) spectral regions are shown for the initial graphene surface on silicon oxide (top), PBSE-modified graphene (middle), and PBSE-modified graphene after immobilization of the simulated DNA probes (bottom). Symbols=raw data; thick lines=overall fits; thin colored lines=fit components; dashed lines=background. The high sensitivity of XPS results in detecting in the N 1s region the small amount of contamination, most likely from polymeric residue, on the initial graphene surface.

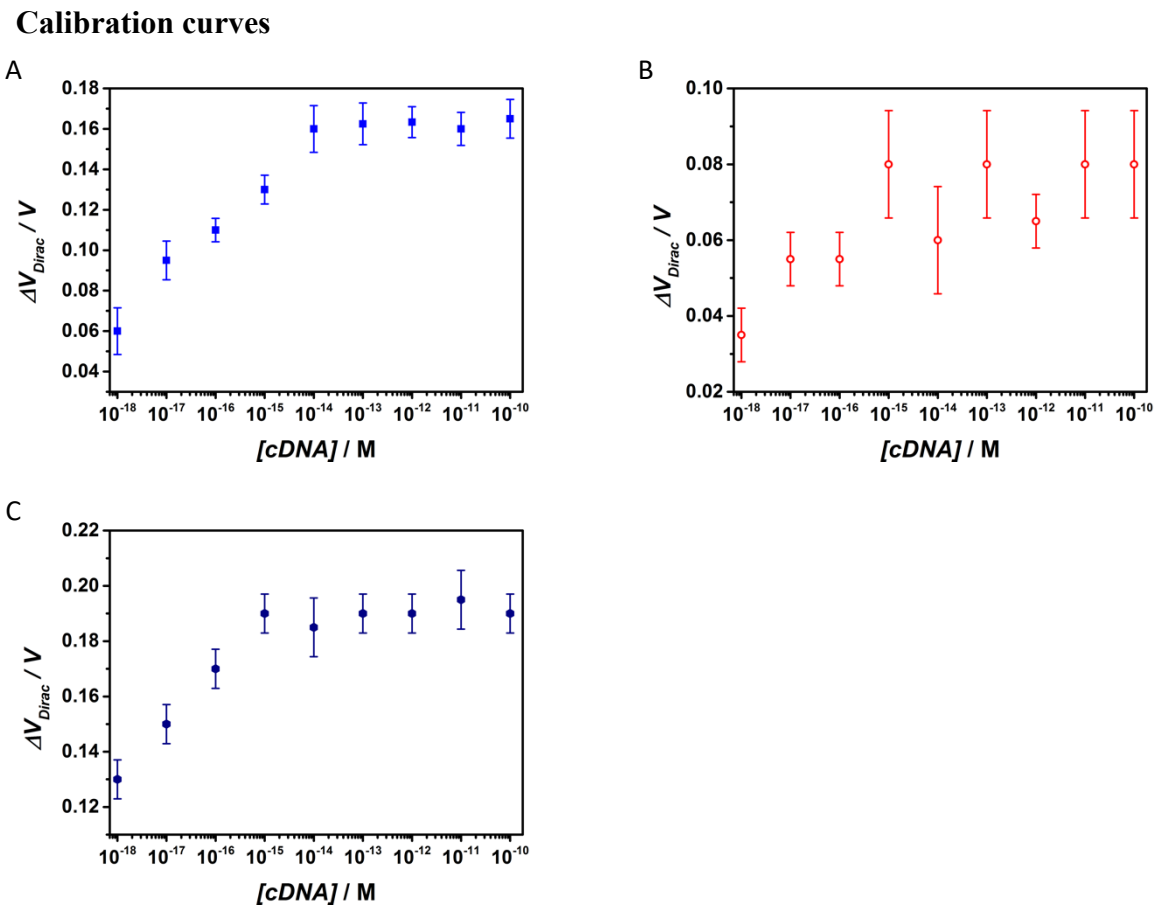

Figure S6 – Calibration curves for the different experiments. A) PM, B) SNP and C) an experiment whose probe DNA was fully complementary to the target named SNP.

Schematic illustration of the molecular system immobilized on graphene, after biorecognition

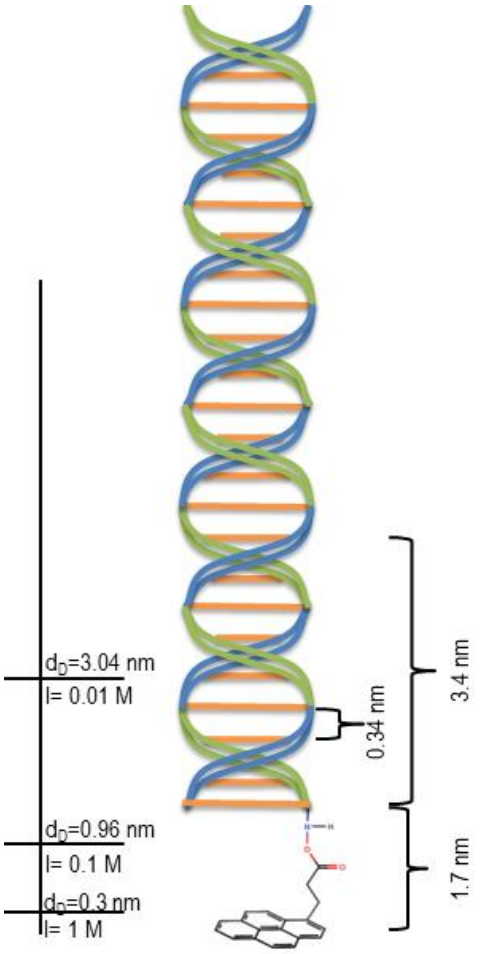

Figure S7. Schematic illustration of a DNA double helix bound to a PBSE linker that links to graphene. Left scale shows Debye length, d_D, as a function of electrolyte ionic strength calculated by Debye-Hückel theory. Right scale shows characteristic molecular lengths.

SEM images of the graphene source, drain and channel area after each biosensor development step

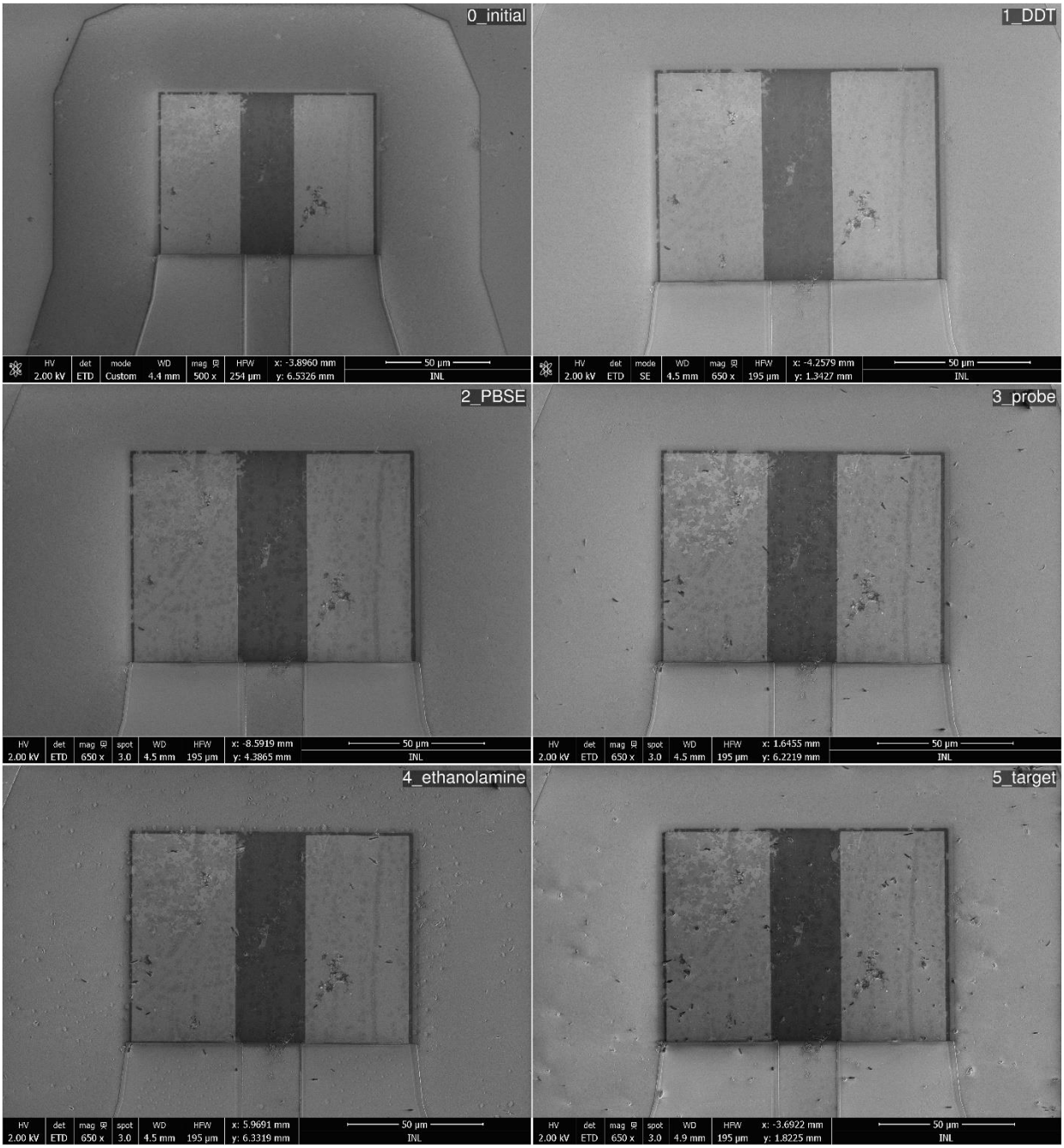

Figure S8 – SEM images of the graphene channel (dark area) of one transistor, in between source and drain Au contacts (clear areas), taken after each of the stages of the biosensor development (see main text and Figure S1). Note that the graphene overlaps the Au S-D contacts, exceeding a few micrometers the Au contact (dark edge). Note: the rectangular source and drain contacts in the images above are slightly different in shape from those shown in the main text (semi-circular).

References

(1) Ferrari, A. C.; Meyer, J. C.; Scardaci, V.; Casiraghi, C.; Lazzeri, M.; Mauri, F.; Piscanec, S.; Jiang, D.; Novoselov, K. S.; Roth, S.; et al. Raman Spectrum of Graphene and Graphene Layers. *Phys. Rev. Lett.* **2006**, *97* (18), 187401 DOI:10.1103/PhysRevLett.97.187401.

(2) Saito, R.; Dresselhaus, G.; Dresselhaus, M. S. *Physical Properties of Carbon Nanotubes*; Published by Imperial College Press and Distributed by World Scientific Publishing Co., 1998.

(3) Shinohara, H.; Yamakita, Y.; Ohno, K. Raman Spectra of Polycyclic Aromatic Hydrocarbons. Comparison of Calculated Raman Intensity Distributions with Observed Spectra for Naphthalene, Anthracene, Pyrene, and Perylene. *J. Mol. Struct.* **1998**, *442* (1–3), 221–234.

(4) Lu, G.; Shi, G. Electrochemical Polymerization of Pyrene in the Electrolyte of Boron Trifluoride Diethyl Etherate Containing Trifluoroacetic Acid and Polyethylene Glycol Oligomer. *J. Electroanal. Chem.* **2006**, *586* (2), 154–160.

(5) Leyton, P.; Gómez-Jeria, J. S.; Sanchez-Cortes, S.; Domingo, C.; Campos-Vallette, M. Carbon Nanotube Bundles as Molecular Assemblies for the Detection of Polycyclic Aromatic Hydrocarbons: Surface-Enhanced Resonance Raman Spectroscopy and Theoretical Studies. *J. Phys. Chem. B* **2006**, *110* (13), 6470–6474.